Journal of Molecular and Cellular Cardiology 60 (2013) 172–183

Contents lists available at SciVerse ScienceDirect

Journal of Molecular and Cellular Cardiology

journal homepage: www.elsevier.com/locate/yjmcc

Original article

Role of CaMKII in post acidosis arrhythmias: A simulation study using a human myocyte model ☆

Elena C. Lascano [a,*], Matilde Said [b], Leticia Vittone [b], Alicia Mattiazzi [b], Cecilia Mundiña-Weilenmann [b], Jorge A. Negroni [a]

[a] Department of Biology, Universidad Favaloro, Buenos Aires, Argentina
[b] Centro de Investigaciones Cardiovasculares, CONICET-La Plata, Facultad de Ciencias Médicas, Universidad Nacional de La Plata, La Plata, Argentina

ARTICLE INFO

Article history:
Received 18 December 2012
Received in revised form 15 March 2013
Accepted 15 April 2013
Available online 23 April 2013

Keywords:
Myocyte model
Post acidotic arrhythmogenesis
Sarcoplasmic reticulum Ca^{2+} leak
CaMKII

ABSTRACT

Postacidotic arrhythmias have been associated to increased sarcoplasmic reticulum (SR) Ca^{2+} load and Ca^{2+}/calmodulin-dependent protein kinase II (CaMKII) activation. However, the molecular mechanisms underlying these arrhythmias are still unclear. To better understand this process, acidosis produced by CO_2 increase from 5% to 30%, resulting in intracellular pH (pH_i) change from 7.15 to 6.7, was incorporated into a myocyte model of excitation-contraction coupling and contractility, including acidotic inhibition of L-type Ca^{2+} channel (I_{CaL}), Na^+–Ca^{2+} exchanger, Ca^{2+} release through the SR ryanodine receptor (RyR2) (I_{rel}), Ca^{2+} reuptake by the SR Ca^{2+} ATPase2a (I_{up}), Na^+–K^+ pump, K^+ efflux through the inward rectifier K^+ channel and the transient outward K^+ flow (I_{to}) together with increased activity of the Na^+–H^+ exchanger (I_{NHE}). Simulated CaMKII regulation affecting I_{rel}, I_{up}, I_{CaL}, I_{NHE} and I_{to} was introduced in the model to partially compensate the acidosis outcome. Late Na^+ current increase by CaMKII was also incorporated. Using this scheme and assuming that diastolic Ca^{2+} leak through the RyR2 was modulated by the resting state of this channel and the difference between SR and dyadic cleft [Ca^{2+}], postacidotic delayed after depolarizations (DADs) were triggered upon returning to normal pH_i after 6 min acidosis. The model showed that DADs depend on SR Ca^{2+} load and on increased Ca^{2+} leak through RyR2. This postacidotic arrhythmogenic pattern relies mainly on CaMKII effect on I_{CaL} and I_{up}, since its individual elimination produced the highest DAD reduction. The model further revealed that during the return to normal pH_i, DADs are fully determined by SR Ca^{2+} load at the end of acidosis. Thereafter, DADs are maintained by SR Ca^{2+} reloading by Ca^{2+} influx through the reverse NCX mode during the time period in which $[Na^+]_i$ is elevated.

1. Introduction

Cardiac muscle becomes acidic in a number of pathological conditions. Acidosis affects myofilament Ca^{2+} responsiveness as well as different processes of excitation-contraction coupling, including sarcolemmal and sarcoplasmic reticulum (SR) ion flows [1–5]. These alterations decrease myocardial contractility and predispose to arrhythmias [6]. Interestingly, in different animal models, the return to normal pH after a period of acidosis is particularly prone to arrhythmias that may evolve to ventricular tachycardia and fibrillation [7–9]. This is important in the scenario of ischemia/reperfusion injury, as intracellular acidosis is a typical component of ischemia and a sudden recovery of pH takes place upon reperfusion.

In the progression of acidosis there are different steps. Early during acidosis, Ca^{2+} myofilament sensitivity decreases [1,2] whereas systolic Ca^{2+} may increase [10,11], decrease [12] or not change [3]. This is followed by a gradual rise in intracellular Ca^{2+} concentration which is responsible for partial recovery of contraction that occurs in spite of the persistent acidosis [8,13,14]. Reduced pH also produces an increased activity of the Na^+–H^+ exchanger (NHE) [15] and reduced Na^+–K^+ pump (NaK) activity [16], increasing intracellular Na^+ concentration [17]. Moreover, acidosis depresses numerous ion flows: Ca^{2+} input through the voltage-dependent L-type Ca^{2+} channel [18], Ca^{2+} release through the SR ryanodine receptor (RyR2) [19], Ca^{2+} reuptake by the sarco(endo)plasmic reticulum Ca^{2+} ATPase2a (SERCA2a) [2], Ca^{2+} extrusion through the Na^+–Ca^{2+} exchanger (NCX) [20], and K^+ efflux through the inward rectifier K^+ channel [21] and the transient outward current [22]. An increase in Ca^{2+}/calmodulin-dependent protein kinase II (CaMKII) activity has also been described during acidosis [6]. Different types of experimental evidence indicate that the activity of this kinase may compensate for the deleterious effect of reduced pH, almost totally in the case of the L-type Ca^{2+} channel [4] and partially on SERCA2a by inducing

☆ This research was supported by ANPCyT (PICT08-0340 to EL and JN), PIP 2139 CONICET to AM and ANPCyT (PICT Nº 2634 to C M-W).

* Corresponding author at: Department of Biology, Universidad Favaloro, Solís 453, (1078) Buenos Aires, Argentina. Tel.: +54 11 4378 1187; fax: +54 11 4381 0323.
E-mail address: elascano@favaloro.edu.ar (E.C. Lascano).

0022-2828/$ – see front matter © 2013 Elsevier Ltd. All rights reserved.
http://dx.doi.org/10.1016/j.yjmcc.2013.04.018

an increase in the phosphorylation of its regulatory protein, phospholamban (PLN) [8,14]. CaMKII has also been shown to phosphorylate the RyR2 [23,24] although this phosphorylation does not attain significant relevance during acidosis [6]. In addition, CaMKII further stimulates NHE activity at low pH [25] and increases the transient outward current [26] and the late Na^+ current [27].

Experimental evidence suggests that postacidotic arrhythmias are mainly triggered by delayed after depolarizations (DADs). DADs would be caused by increased NCX activity in response to Ca^{2+} leak from an overloaded SR due to CaMKII-dependent increase in SR Ca^{2+} uptake [6]. SR Ca^{2+} leak would be also favored by the relief of the RyR2 previously inhibited by acidosis. However, this hypothesis is still subject to discussion as the analysis of the simultaneous contribution of different ion concentrations and flows to arrhythmia development is difficult to assess experimentally.

A previous myocyte model attempted to explain the significance of the mechanisms involved in acidosis [28]. In this model, the acidotic impairing effect on ion flows and contractility together with a compensatory role of CaMKII on L-type Ca^{2+} channel and SERCA2a were able to predict the time course of changes in intracellular Na^+, cytosolic and SR Ca^{2+} concentrations and force due to pH variation, but it did not reproduce postacidotic arrhythmias. The purpose of this study was thus to develop a myocyte model of acidosis to represent the effects of intracellular acidosis both on contractility and spontaneous depolarizations, analyzing the contribution of ion flows and the role of CaMKII in the generation of postacidotic arrhythmias. A modified human myocyte model [29] was then used with contractility based on a previous mechanical model consisting of sarcomere dynamics coupled to Ca^{2+} kinetics [30], and acidosis and CaMKII effects on ion flows and contractile constants.

The present mechanistic model supports previous experimental data indicating that the arrhythmogenic pattern observed after acidosis is greatly dependent on the effects of CaMKII on sarcolemmal and intracellular targets. The model further establishes that postacidotic arrhythmias depend on SR Ca^{2+} leak which is mainly triggered by a loaded SR during the return to normal pH. Once SR load has attained preacidotic values, arrhythmic episodes are maintained by SR Ca^{2+} reloading due to the increased NCX activity during the period in which intracellular Na^+ is elevated.

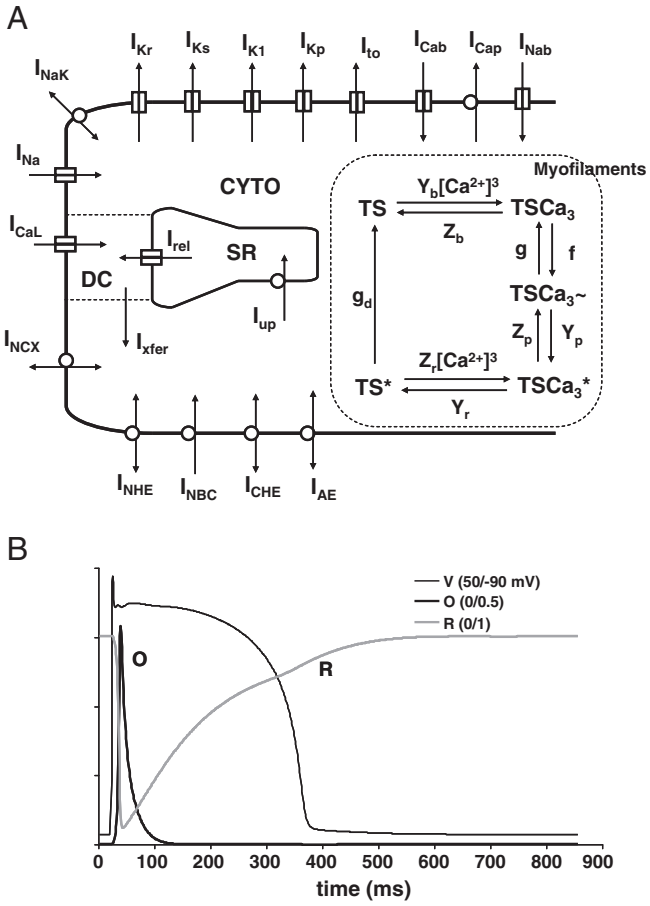

Fig. 1. Schematic diagram of the model and RyR2 kinetic behavior. *A*: Human myocyte model consisting of ion pumps and exchangers responsible for action potential, Ca^{2+} management, force development and pH_i regulation. *B*: Model-derived time course of action potential and open (O) and resting (R) RyR2 states, respectively determining $I_{release}$ and I_{leak}. See Non-standard abbreviations.

2. Methods

The human epicardial ventricular myocyte ion flow model postulated by ten Tusscher & Panfilov (TP) was used [29]. This model describes three compartments: dyadic cleft (DC), SR and cytoplasm (CYTO), (Fig. 1A). A contractile component was incorporated based on a previous sarcomere model [30] in which total muscle force (F_m) is equal to cross-bridge (F_b) plus parallel elastic forces (F_p). Simplification of the model reducing the number of Ca^{2+} binding troponin systems (TS) from six to five did not affect its reported performance (see Supplementary Material for model equations and parameter values). Each TS is composed of 3 adjacent troponin-tropomyosin regulatory units acting cooperatively: free TS; Ca^{2+} bound to TS without attached crossbridges ($TSCa_3$), Ca^{2+} bound to TS with attached crossbridges in the weak state ($TSCa_3$~), Ca^{2+} bound to TS with attached crossbridges in the power state ($TSCa_3$*), and TS without Ca^{2+} with attached crossbridges in the power state (TS*).

Ca^{2+}-induced- Ca^{2+} release flow ($I_{release}$) into the DC through RyR2 was based on the 4-state Shannon model also employed by ten Tusscher et al. (29), with open (O), closed (R) and intermediate probability states [31]. According to this representation, Ca^{2+} release depends on the open state (O) of RyR2 [29,31] as follows:

$$I_{release} = V_{rel}.O.\left(\left[Ca^{2+}\right]_{SR} - \left[Ca^{2+}\right]_c\right)$$

where V_{rel} is $I_{release}$ rate constant, $[Ca^{2+}]_{SR}$ is SR Ca^{2+} concentration and $[Ca^{2+}]_c$ is DC Ca^{2+} concentration.

However, different from other models where SR Ca^{2+} leak was built as a separate entity from RyR2 with constant rate parameters toward either CYTO [29] or DC [31], SR Ca^{2+} leak was represented as Ca^{2+} flow through RyR2 (I_{leak}) modulated by the R state of this channel:

$$I_{leak} = V_{sp}.R.\left(\left[Ca^{2+}\right]_{SR} - \left[Ca^{2+}\right]_c\right)$$

where V_{sp} is I_{leak} rate constant. Thus, the combination of both $I_{release}$ and I_{leak} participate in a single release flow (I_{rel}) from RyR2 (Fig. 1B):

$$I_{rel} = I_{release} + I_{leak} = \left(V_{rel}.O + V_{sp}.R\right).\left(\left[Ca^{2+}\right]_{SR} - \left[Ca^{2+}\right]_c\right)$$

with $V_{rel} = 0.102$ 1/ms and $V_{sp} = 0.00036$ 1/ms, as well as the rest of RyR2 parameters and buffers employed by ten Tusscher [29] because they satisfied a suitable I_{rel} performance. Effectively, end stabilization I_{leak} extrapolated at model $[Ca^{2+}]_{SR}$ from the experimental relationship reported by Shannon et al. [32], was lower than expected (52 vs. 73 μmol/L CYTO/s).

CaMKII was activated according to the model and using the same parameters postulated by Chiba [33], except that the sequential four-step Ca^{2+} binding to calmodulin was reduced to one step. Its effect on L-type Ca^{2+} channel (I_{CaL}), RyR2 receptor (I_{rel}), SERCA2a (I_{up}),

transient outward current (I_{to}), NHE (I_{NHE}), and late Na^+ current (late I_{Na}) flows was described as

$$I = (1-\Phi).I_b + \Phi.I_{CaMKII} \quad (1)$$

where I is total flow, I_b is basal flow without CaMKII activation, Φ is fraction of activated channels (or transporters) and I_{CaMKII} is flow with CaMKII activation. Accepting

$$I_{CaMKII} = I_b + \Delta I_b$$

where ΔI_b is the increase in flow due to CaMKII activation, substitution into Eq. (1) results as:

$$I = I_b(1 + \Phi.\Delta I_b/I_b)$$

with CaMKII factor $fe = (1 + \Phi.\Delta I_b/I_b)$, where $\Delta I_b/I_b = IF_{CaMKII}$ is increased flow fraction produced by CaMKII activation. Then,

$$I = fe.\ I_b \quad (2)$$

Since according to O'Hara [34] $\Phi = 1/(1 + K_{mCaMKII}/CaMKII_{act})$, where $K_{mCaMKII}$ is constant and $CaMKII_{act}$ is fraction of activated CaMKII, then:

$$fe = 1 + \frac{IF_{CaMKII}}{1 + \frac{K_{mCaMKII}}{CaMKII_{act}}}$$

For *fe* calculation, mean IF_{CaMKII} was 0.25 for I_{CaL} [34], 0.05 for I_{rel}, (to fit experimental data, [6], 0.45 for I_{up} (model fit), 0.2 for I_{NHE} [25], 0.08 for I_{to} [34], and 0.2 for late I_{Na} [27].

Intracellular pH (pH_i) was determined by extracellular CO_2 according to ionic changes established by H^+–HCO_3^- formation, and regulated by Na^+–HCO_3^- cotransporter (I_{NBC}), Cl^-–OH^- (I_{CHE}), Cl^-–HCO_3^- (I_{AE}) and I_{NHE} exchanger flows and intracellular pH_i buffers [28]. Increase from 5% to 30% CO_2 reduced pH_i from 7.15 to approximately 6.7. Acidosis-induced reduction of I_{CaL}, I_{rel}, I_{up}, I_{to}, I_{AE}, NCX (I_{NCX}), NaK (I_{NaK}) and the inward rectifier K^+ channel (I_{K1}) flows, and PP1 activity [35] together with increase of I_{NHE}, I_{NBC}, and contractile constants, were fitted to a sigmoidal relationship [28], described by the following general pH_i factor (*fh*):

$$fh = \frac{f_0}{1 + 10^{n(-pH_i+pK)}}$$

where f_0, n and pK are *fh* parameters. Table A1 in the Appendix A shows *fh* parameters fitted according to the indicated reference for the different pH_i targets.

To maintain the TP model structure, f_0 was assigned different values on each pH_i target to obtain $fh = 1$ at $pH_i = 7.15$.

Incorporating *fh* into Eq. (2), results in

$$I = fe.fh.\ I_b$$

that takes into account both $CaMKII_{act}$ and pH_i effects on the corresponding ion flows.

2.1. Simulations

Simulations were performed at a constant pacing frequency (PF) of 70 stimuli/min. All variables were stable during the whole simulation period at constant 5% CO_2, varying <0.01% among twitches (Figure SM1 in Supplementary Material). Thus, at the end of the stabilization at 5% CO_2 all the variables showed the expected profiles (Figure SM2). This was followed by acidosis, achieved with 30% CO_2 producing a gradual decrease in $pH_i = 6.7$, and sustained during a 6 min acidotic period. Then, the return to 5% CO_2 led to a gradual return to preacidotic pH_i which was maintained for another 5 min (post acidosis).

This procedure was used in the following protocols:

S1: Simulation of acidosis affecting contractile constants, PP1 and I_{rel}, I_{up}, I_{CaL}, I_{NCX}, I_{NHE}, I_{AE}, I_{NBC},I_{NaK}, I_{K1}, and I_{to} with CaMKII activation on I_{rel}, I_{up}, I_{CaL}, I_{NHE}, I_{to} and late I_{Na} flows.
S1-SRb: Simulation as in S1 with the SR function blocked using a constant open probability value of 0.7 and dividing maximal I_{up} by 10.

To analyze the impact of changes in frequency and acidosis duration on DAD generation, different PFs (±10 stimuli/min) and periods of acidosis (±50%) were tested in the same conditions as S1:

S1–60: Simulation as in S1 at 60 stimuli/min.
S1–80: Simulation as in S1 at 80 stimuli/min.
S1–3 m: Simulation as in S1 with 3 min acidosis duration.
S1–9 m: Simulation as in S1 with 9 min acidosis duration.
S2: Simulation of acidosis as in S1 without CaMKII effects on I_{rel}, I_{up}, I_{CaL}, I_{NHE}, I_{to} and late I_{Na}.
S3: Simulation of acidosis as in S1 without CaMKII effect on I_{rel}.
S4: Simulation of acidosis as in S1 without CaMKII effect on I_{CaL}.
S5: Simulation of acidosis as in S1 without CaMKII effect on I_{up}.
S6: Simulation of acidosis as in S1 without CaMKII effect on I_{NHE}.
S7: Simulation of acidosis as in S1 without CaMKII effect on late I_{Na}.
S8: Simulation of acidosis as in S1 without CaMKII effect on I_{to}.

The model code was developed in MATLAB using ODE15s solver. Units were: ms for time, μm for length, μM for concentration, A/F for sarcolemmal flows, μM/ms for intracellular flows, mV for potential and mN/mm^2 for force.

2.1.1. Heart perfusion experiments

Experiments were performed in transgenic mice (25–30 g) with genetic ablation of PLN (PLN-KO) [36]. Isolated hearts were perfused according to Langendorff technique and mechanical parameters and monophasic action potentials were obtained as previously described [6]. Hearts were perfused in the absence and presence of 100 nM thapsigargin or 100 nM thapsigargin plus 5 μM monensin. Quantification of spontaneous activity was accomplished by counting the number of beats occurring between triggered electrical activity during a period of 3 min after drug addition.

Statistics. Data are expressed as mean ± SEM. ANOVA followed by the Newman-Keuls test was used to determine statistical significance. A p value < 0.05 was considered statistically significant.

3. Results

3.1. Model behavior under acidotic and postacidotic conditions

Fig. 2A (upper panel) illustrates F_m behavior in the S1 protocol during acidosis and the return to normal pH_i. At the onset of acidosis there was an abrupt decrease of F_m followed by a rapid and partial recovery throughout the duration of the acidotic period. Upon returning to normal pH_i, F_m showed an arrhythmic pattern. To assess the extent to which our model could predict experimental behavior, we compared model predictions with available experimental data. As shown in the lower panel of Fig. 2A, the model accurately reproduced developed pressure data of an isolated rat heart submitted to a similar protocol [6]. In the model (Fig. 2B), an increase in CO_2 from 5% to 30% decreased pH_i to a minimum 6.7, which tended to recover during the acidotic period and then returned toward its normal value upon 5% CO_2 restitution. The decrease in pH_i produced a fast increase in maximum CYTO $[Ca^{2+}]$, ($[Ca^{2+}]_i(max)$) and maximum SR $[Ca^{2+}]$, ($[Ca^{2+}]_{SR}(max)$), which was maintained during the 6 min acidosis. Concomitantly, $[Ca^{2+}]$/twitch exchanged through NCX decreased at

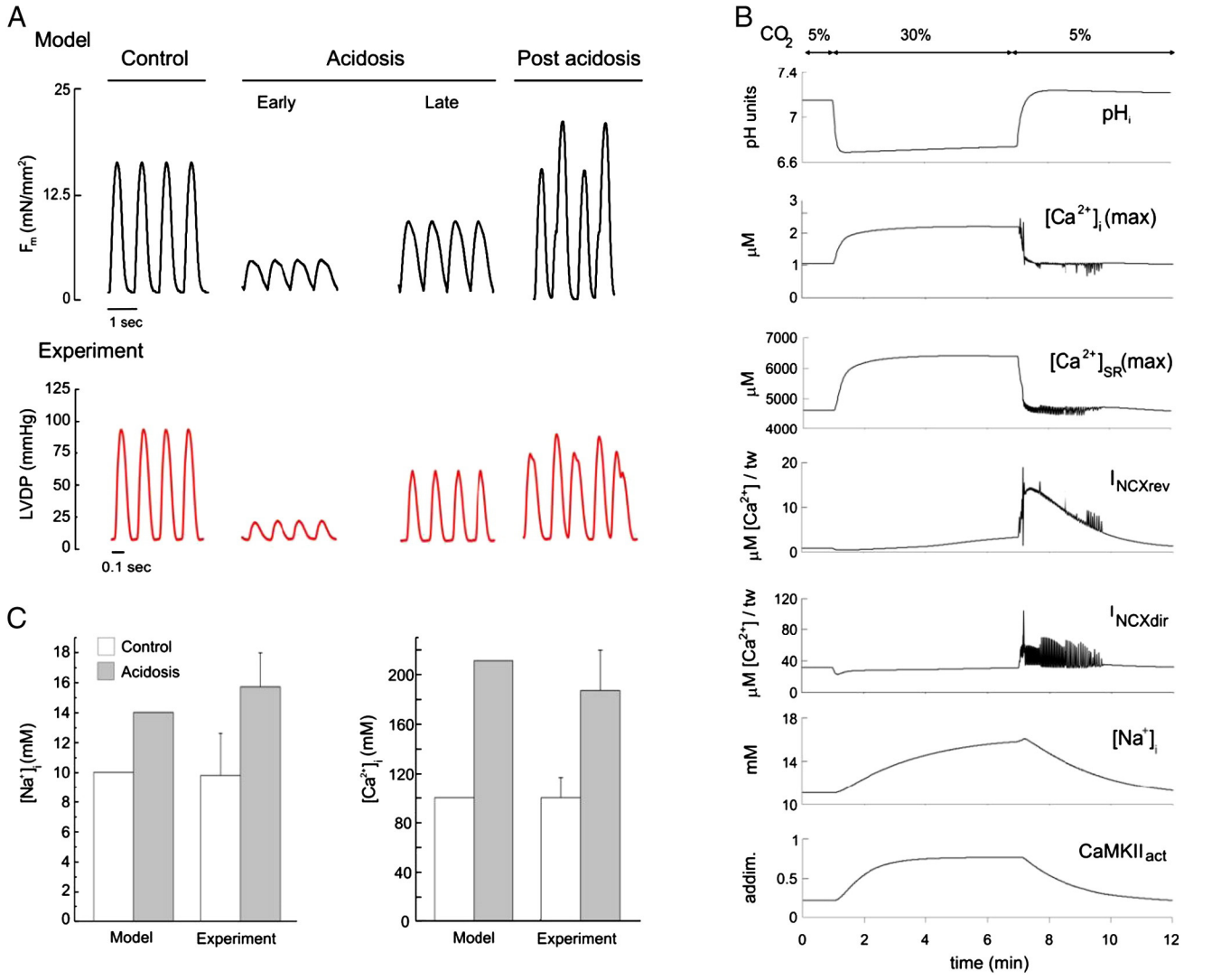

Fig. 2. Acidosis and return to normal pH_i in the S1 protocol. *A*: Comparison of records of model developed force (F_m) (PF = 70 stimuli/min) and left ventricular developed pressure (LVDP, PF = 240 beats/min) of a Langendorff perfused rat heart obtained from previous experiments from Said et al. [6] during control, early and late acidosis and post acidosis. *B*: pH_i behavior, maximum twitch values of $[Ca^{2+}]_i$ ($[Ca^{2+}]_i$(max)), $[Ca^{2+}]_{SR}$ ($[Ca^{2+}]_{SR}$(max)), total Ca^{2+} exchanged (μmol/twitch/L CYTO/s) through the reverse and direct modes of the NCX (I_{NCXrev} and I_{NCXdir}), mean $[Na^+]_i$ and mean activated CaMKII/twitch ($CaMKII_{act}$) due to CO_2 changes. For clarity, only one value per twitch is shown. ***C*:** Comparison of model and experimental $[Na^+]_i$ and $[Ca^{+2}]_i$ transient amplitude during control and at the end of acidosis (data from Perez et al. for $[Na^+]_i$ [36] and Nomura et al. for $[Ca^{+2}]_i$ [8]. The Figure shows that the model reproduced experimentally obtained arrhythmias (*A*) and the increase in $[Na^+]_i$ and $[Ca^{2+}]_i$ (*C*).

the beginning of acidosis and then recovered, gradually in the case of the reverse mode flow (I_{NCXrev}) and immediately in that of the direct mode flow (I_{NCXdir}). $[Na^+]$ in CYTO ($[Na^+]_i$) and $CaMKII_{act}$, both showed a consistent rise throughout the duration of acidosis. In association with the F_m postacidotic arrhythmic pattern, instability in $[Ca^{2+}]_i$(max), $[Ca^{2+}]_{SR}$(max) and in the activity of both I_{NCXdir} and I_{NCXrev} was observed. This occurred with the concomitant abrupt decrease of $[Ca^{2+}]_i$(max) and $[Ca^{2+}]_{SR}$(max), and the gradual fall of I_{NCXrev}, $[Na^+]_i$ and $CaMKII_{act}$ toward preacidotic values. Simulated acidosis effects were confirmed by acceptable agreement between experimental and model results of $[Ca^{2+}]_i$ [8] and $[Na^+]_i$ [37] at the end of the acidotic period (Fig. 2C). Table 1 also shows that $[Ca^{2+}]_i$(max), $[Ca^{2+}]_{SR}$(max) and $[Na^+]_i$ values at the end of 6 min acidosis (A) increased with respect to basal preacidotic normal twitches (B), maximum F_m [F_m(max)] decreased and action potential (AP) duration at 90% repolarization (APD_{90}) increased 7% at the beginning of acidosis and then returned to a 2% increase at the end of the acidotic period, showing a similar behavior to that experimentally reported in the mammalian heart [38].

Fig. 3 illustrates DAD generating events. Fig. 3A shows membrane potential (V) and $[Ca^{2+}]_{SR}$ of the first seconds upon returning to 5% CO_2. DADs, which can be better appreciated in an expanded time scale (Figs. 3F and H) could be observed throughout this period. DADs were able to trigger spontaneous APs (DAD_{AP}) mostly during early post acidosis, which is the period between the return to 5% CO2 and pH_i recovery to near steady preacidotic values, a period which is almost coincident with $[Ca^{2+}]_{SR}$ restitution from high Ca^{2+} load. Once $[Ca^{2+}]_{SR}$ reached preacidotic values, DADs were progressively unable to attain the threshold to trigger DAD_{AP}, generating subthreshold DADs (DAD_{ST}) during late post acidosis. Figs. 3B to E show in an expanded time scale that DAD_{AP} occurred associated with Ca^{2+} influx through the L-type Ca^{2+} channels (I_{CaL}), an increase in $[Ca^{2+}]_c$ and Ca^{2+}-induced-Ca^{2+} release, enhancing I_{rel}, as in the stimulated AP. However, in contrast to what occurs in the stimulated AP, in the DAD_{AP}, the activity of I_{NCX} was markedly increased. Moreover, DAD_{AP} developed F_m aftercontractions, which occurred before the preceding twitch had attained complete relaxation, altering the normal mechanical activity of the cell. Notice that DAD_{ST} developed without

Table 1
Ca^{2+} and Na^{+} concentrations, peak force and AP duration in basal (B) and at the end of 6 min acidosis (A), with CAMKII effect on specific flows.

Protocol	CaMKII action		$[Ca^{2+}]_i$(max) (μM)	$[Ca^{2+}]_i$(min) (μM)	$[Ca^{2+}]_{SR}$ (max) (μM)	$[Na^{+}]_i$ (mM)	F (max) (mN/mm^2)	APD_{90} (ms)
S1	I_{rel}, I_{up}, I_{CaL}, I_{NHE}, I_{to}, late I_{Na}	B	1.021	0.118	4598	10.77	13.64	343
		A	2.155	0.168	6451	15.21	7.67	350
S1-SRb	I_{rel}, I_{up}, I_{CaL}, I_{NHE}, I_{to}, late I_{Na}	B	0.456	0.190	446	13.59	4.50	311
(SR blocked)		A	0.947	0.444	787	19.02	3.25	298
S1–60	I_{rel}, I_{up}, I_{CaL}, I_{NHE}, I_{to}, late I_{Na}	B	0.889	0.103	4154	10.01	10.89	349
(PF = 60)		A	1.999	0.149	6277	14.23	6.95	357
S1–80	I_{rel}, I_{up}, I_{CaL}, I_{NHE}, I_{to}, late I_{Na}	B	1.098	0.145	4821	11.31	15.13	335
(PF = 80)		A	2.277	0.190	6509	15.97	8.39	341
S1–3 m	I_{rel}, I_{up}, I_{CaL}, I_{NHE}, I_{to}, late I_{Na}	B						
(AD = 3 min)		A	2.155	0.158	6470	14.04	5.78	357
S1–9 m	I_{rel}, I_{up}, I_{CaL}, I_{NHE}, I_{to}, late I_{Na}	B						
(AD = 9 min)		A	2.079	0.172	6340	15.38	9.06	347
S2		B	0.881	0.106	4023	10.47	11.22	341
		A	1.710	0.151	5485	14.57	5.45	341
S3	I_{up}, I_{CaL}, I_{NHE}, I_{to}, late I_{Na}	B	1.026	0.118	4654	10.76	13.75	343
		A	2.165	0.166	6562	15.22	7.72	351
S4	I_{rel}, I_{up}, I_{NHE}, I_{to}, late I_{Na}	B	0.947	0.109	4352	10.33	11.95	340
		A	1.962	0.151	6184	14.41	6.45	343
S5	I_{rel}, I_{CaL}, I_{NHE}, I_{to}, late I_{Na}	B	0.948	0.114	4202	10.97	13.04	345
		A	1.896	0.167	5705	15.59	6.96	348
S6	I_{rel}, I_{up}, I_{CaL}, I_{to}, late I_{Na}	B	1.020	0.118	4595	10.76	13.63	343
		A	2.157	0.167	6456	15.11	7.46	351
S7	I_{rel}, I_{up}, I_{CaL}, I_{NHE}, I_{to},	B	1.019	0.118	4591	10.75	13.60	343
		A	2.150	0.167	6444	15.19	7.63	349
S8	I_{rel}, I_{up}, I_{CaL}, I_{NHE}, late I_{Na}	B	1.019	0.116	4592	10.75	13.61	343
		A	2.151	0.168	6445	15.19	7.64	349

$[Ca^{2+}]_i$(max):maximum and $[Ca^{2+}]_i$(min): minimum intracellular Ca^{2+} concentrations, $[Ca^{2+}]_{SR}$ (max): maximum SR Ca^{2+} concentration, $[Na^{+}]_i$: intracellular Na^{+} concentration, F (max): maximum force and APD_{90}: action potential duration at 90% repolarization. AD: acidosis duration. S1–S8: acidosis on I_{rel}, I_{up}, I_{CaL}, I_{NCX}, I_{NHE}, late I_{Na}, I_{K1}, I_{NaK} and I_{to} with CaMKII effect as indicated in the different protocols. Acidosis effect on contractile constants is the same in all protocols. See Glossary for abbreviations. See Methods for protocol specifications.

contribution of extracellular Ca^{2+} as indicated by the absence of I_{CaL}. All these changes and their temporal sequence are better appreciated in Figs. 3F to I. Figs. 3F and G show that while in the stimulated twitch the simultaneous upstroke of AP, activation of I_{Na}, I_{NCXrev}, and I_{CaL} preceded the increase in $[Ca^{2+}]_c$ and I_{rel}, in DAD_{AP} this sequence changed. In this case, the increase in $[Ca^{2+}]_c$ and I_{rel} leading to increased $[Ca^{2+}]_i$ and therefore I_{NCXdir}, preceded membrane depolarization up to the level of fast Na^{+} channel opening (I_{Na}), I_{CaL} and DAD_{AP}. Figs. 3H and I show that when $[Ca^{2+}]_{SR}$ returned to near basal values (Fig. 3A), the same sequence of events elicited a DAD_{ST} instead of DAD_{AP}. This was due to the lower rise in $[Ca^{2+}]_c$, which by inducing less I_{rel} precluded I_{Na} and I_{CaL} that provoked a DAD_{AP}. In this case, lack of Na^{+} influx did not produce a fast change to I_{NCXrev}, allowing for a slower decay of I_{NCXdir} activity.

3.2. SR participation in DADs

Fig. 4A shows that the progressive increase in SR Ca^{2+} load was associated with the consistent enhancement in $[Ca^{2+}]_c$ required to activate a DAD. To further test whether the SR function was a requisite to trigger DADs, I_{rel} and I_{up} were blocked considering the O state of the RyR2 equal to 0.7 and dividing maximal I_{up} by 10 in the S1 protocol (S1-SRb). This constant opening of the RyR2 and depression of SERCA2a activity abolished SR function as evidenced by the drastic decrease in $[Ca^{2+}]_{SR}$(max) before acidosis when compared to S1 (Table 1 and Fig. 4B). The model also indicates that $[Ca^{2+}]_{SR}$ and I_{NCXdir} slightly recovered during acidosis, though there was a prominent increase in $[Na^{+}]_i$ associated to I_{NCXrev} enhancement. Under these conditions, the developed F_m showed only a slight improvement during acidosis and upon returning to normal pH_i no spontaneous events were observed in accordance with experimental data (Fig. 4C) [6]. After acidosis, all variables tended to recover to preacidotic levels.

3.3. DAD dependence on PF and the acidotic period

To analyze whether DAD occurrence depended on PF or acidosis duration, the same S1 protocol was performed at 60 (S1–60) and 80 (S1–80) stimuli/min and during 3 (S1–3 m) and 9 min (S1–9 m). While the number of DAD_{AP} was not affected by PF or acidosis duration, the decrease or increase in PF or acidosis duration decreased or increased respectively, the number of DAD_{ST} (Fig. 5A). Moreover, for a similar $[Na^{+}]_i$ level at end acidosis, achieved either with PF or with the duration of acidosis (Table 1), there was a much greater increase in the number of DADs at the shorter acidotic period. Interestingly, this greater number of DADs was associated with a lower rate of $[Na^{+}]_i$ decline during the postacidotic period (Fig. 5B). The arrhythmogenic response to PF in acidotic conditions was supported by the acceptable frequency-dependent behavior of the model at normal pH_i (Figure SM3).

3.4. Role of CaMKII in postacidotic DADs

To examine the putative role of CaMKII on DAD occurrence, simulations were planned eliminating CaMKII effect on I_{rel}, I_{CaL}, I_{up}, I_{NHE}, late I_{Na} and I_{to} during acidosis. When the stimulatory effects of CaMKII were simultaneously abolished in all flows (S2 protocol), a situation that mimics the treatment with KN93 [6], a prominent decrease in F_m was obtained during acidosis, similar to the fall in developed pressure (Fig. 6A). Table 1 and Fig. 6B show that in this condition, $[Ca^{2+}]_i$(max), $[Ca^{2+}]_{SR}$(max) and $CaMKII_{act}$ were lower than S1 at end acidosis. As a consequence I_{NCXdir} did not recover, producing a smaller increase in $[Na^{+}]_i$ and I_{NCXrev} when compared to the S1 protocol. These combined effects resulted in complete abrogation of DADs upon returning from acidosis, as experimentally observed. Moreover, it was possible to differentiate CaMKII dependence of arrhythmic events by separately eliminating CaMKII effects on the different flows (Fig. 6C and Table 1). In fact, DAD_{AP} were observed in all the simulations in which an enhanced

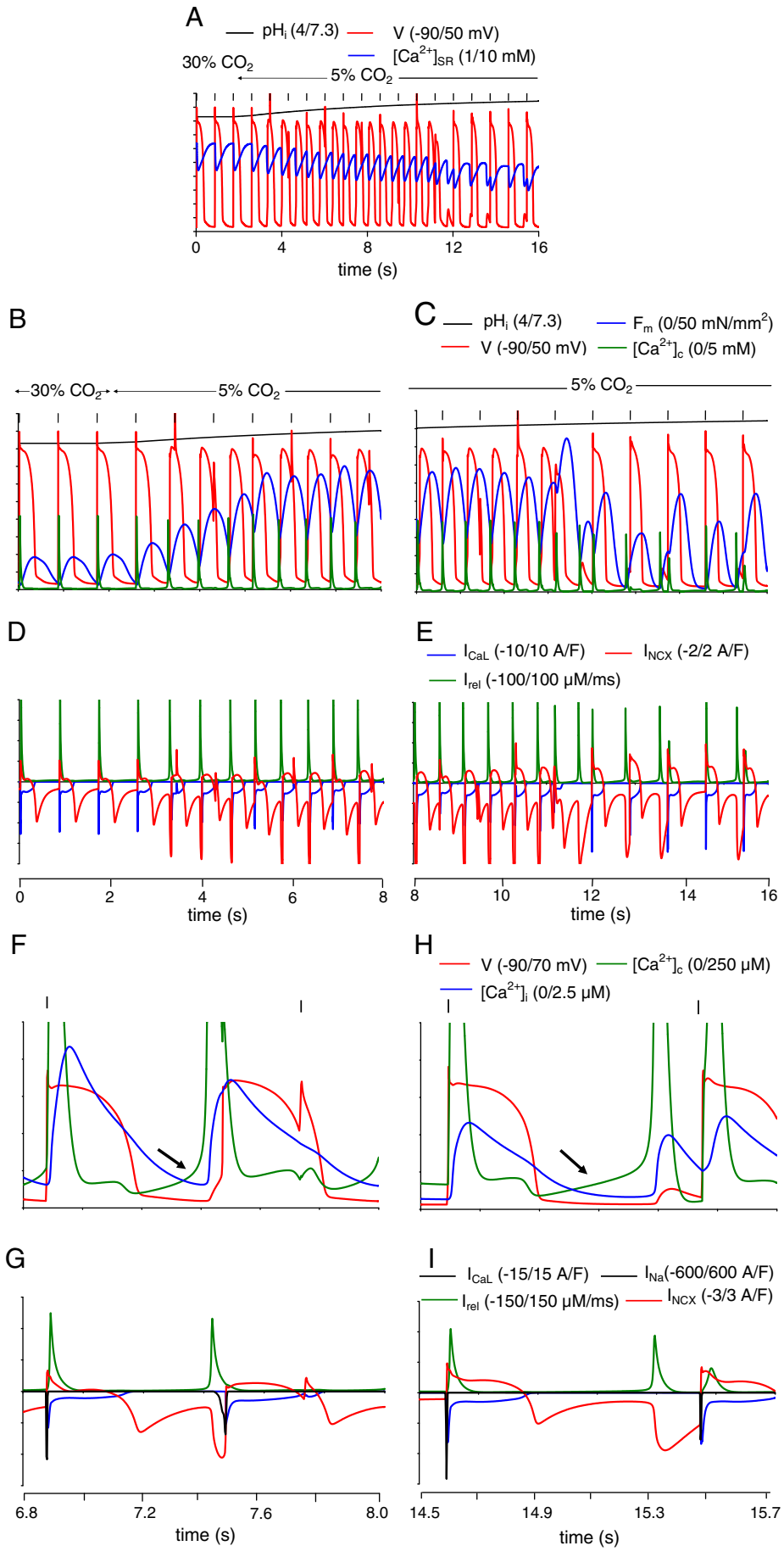
A
pHi (4/7.3)
V (-90/50 mV)
[Ca2+]SR (1/10 mM)
30% CO2
5% CO2
0
4
8
12
16
time (s)
B
30% CO2
5% CO2
C
pHi (4/7.3)
Fm (0/50 mN/mm2)
V (-90/50 mV)
[Ca2+]c (0/5 mM)
5% CO2
D
0
2
4
6
8
time (s)
E
ICaL (-10/10 A/F)
INCX (-2/2 A/F)
Irel (-100/100 µM/ms)
8
10
12
14
16
time (s)
F
H
V (-90/70 mV)
[Ca2+]c (0/250 µM)
[Ca2+]i (0/2.5 µM)
G
6.8
7.2
7.6
8.0
time (s)
I
ICaL (-15/15 A/F)
INa(-600/600 A/F)
Irel (-150/150 µM/ms)
INCX (-3/3 A/F)
14.5
14.9
15.3
15.7
time (s)

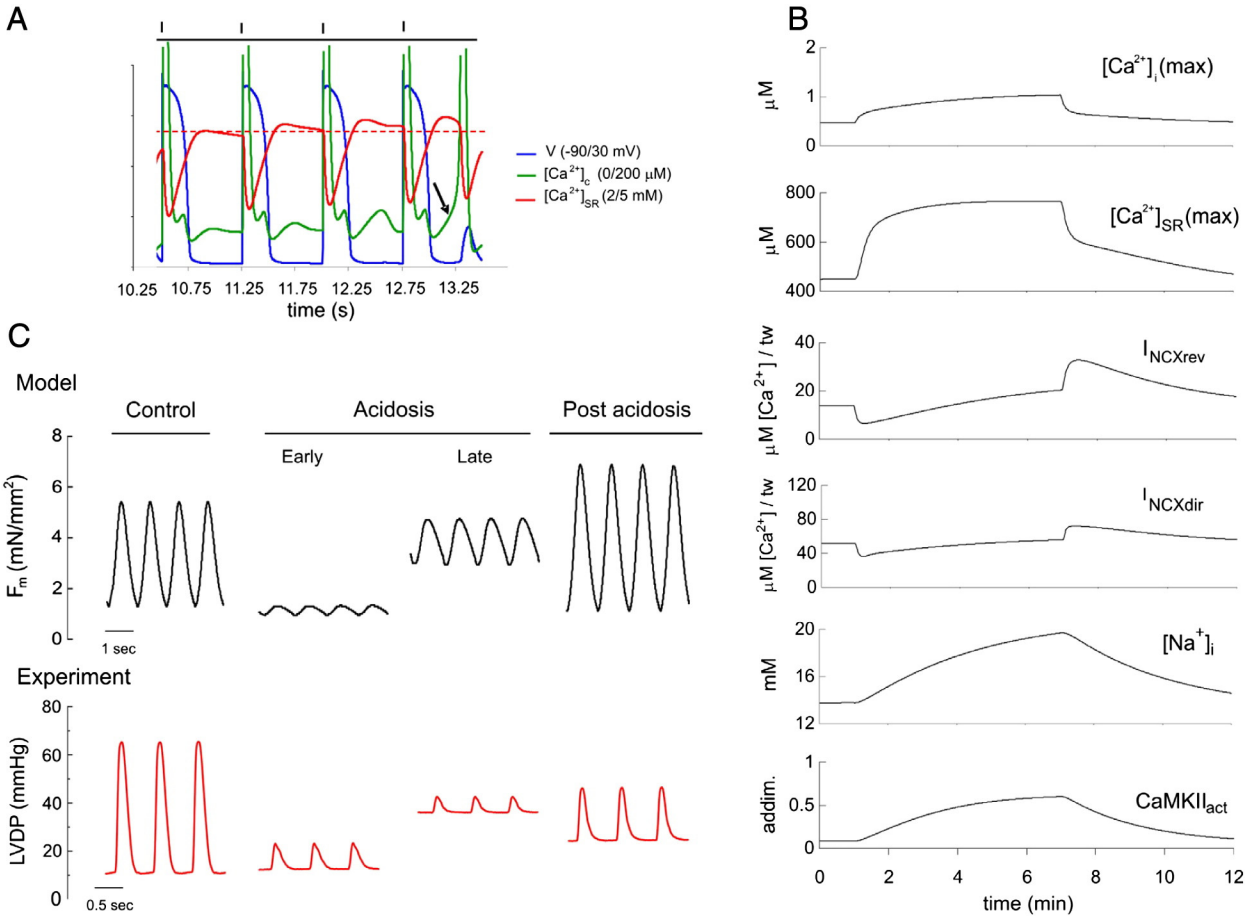

Fig. 4. Role of SR in DAD generation. *A*: Post acidosis twitches in S1, showing action potentials (V) and progressive diastolic rise in $[Ca^{2+}]_{SR}$ accompanied by increasing $[Ca^{2+}]_c$ which finally reaches the level (indicated by the arrow) of generating a DAD_{ST}. Scale range and units are indicated in brackets. *B*: Effect of blocking SR on $[Ca^{2+}]_i$(max), $[Ca^{2+}]_{SR}$(max), I_{NCXrev}, I_{NCXdir}, $[Na^+]_i$ and $CaMKII_{act}$ in the S1-SRb protocol. Despite high $[Na^+]_i$, no DADs are observed probably due to the very low $[Ca^{2+}]_{SR}$ (notice scale difference). *C*: Comparison of records of model developed F_m with blocked SR function (S1-SRb) and LVDP (PF = 120 beats/min) of a Langendorff perfused rat heart in the presence of 30 nM ryanodine obtained from previous experiments from Said et al. [6] during control, early and late acidosis and post acidosis. Abbreviations as in Fig. 2.

$[Ca^{2+}]_{SR}$ was obtained by CaMKII compensation of I_{up} during acidosis (S1, S3, S4, S6, S7 and S8), and not in S2 and S5 in which I_{up} was not protected by CaMKII. In addition, DAD_{ST} were generated when both $[Na^+]_i$ was increased at the end of acidosis and I_{up} was protected by CaMKII. Effectively, in S5 where $[Na^+]_i$ was high but I_{up} was not protected by CaMKII only few DAD_{ST} were elicited.

According to model predictions both an increased SR Ca^{2+} content and $[Na^+]_i$ are necessary for DAD occurrence. In order to test this, we performed experiments in PLN KO mice, in which SR Ca^{2+} load is enhanced due to lack of PLN restriction to SERCA2a (Fig. 6D). Spontaneous beats were scarce in perfused isolated hearts from these mice. In this case, the high SERCA2a activity would be able to deal with excess SR Ca^{2+} leak produced by SR Ca^{2+} overload, precluding arrhythmia generation. When thapsigargin was added in a lower concentration to simulate SERCA2a regulation by PLN (only 40% of the SR Ca^{2+} pump is inhibited by PLN [39]), spontaneous beats increased. A further increase in spontaneous activity occurred when the Na^+ ionophore, monensin, was added. The number of spontaneous beats observed in this latter condition was similar to that observed in WT hearts after the acidosis period [6].

4. Discussion

Cardiac arrhythmias are a leading cause of morbidity and mortality. However, the mechanisms underlying this life-threatening disease are far from being clear [40,41]. Moreover, the multifunctional CaMKII has emerged as an important signaling molecule in the setting of cardiac arrhythmias [42]. This action can be accomplished in different ways.

Fig. 3. Expanded time scale of the S1 protocol upon returning to preacidotic conditions. *A*. Time course of pH_i, membrane potential (V) and $[Ca^{2+}]_{SR}$. During the return to normal pH_i, the overloaded SR triggered DAD_{AP}. Once $[Ca^{2+}]_{SR}$ reached preacidotic values, DAD_{ST} were generated. *B - E*: Expanded time scale of pH_i, V, F_m, $[Ca^{2+}]_c$, I_{CaL}, I_{rel} and I_{NCX} upon returning to preacidotic conditions. *B* and *D* show DAD_{AP} accompanied by summation of developed F_m with concomitant occurrence of I_{CaL}, I_{rel} and increase in $[Ca^{2+}]_c$ and I_{NCXdir}. *C* and *E* show that DAD_{AP} come to an end in association with lower $[Ca^{2+}]_c$. Thereafter, DADs and aftercontractions are generated in the absence of I_{CaL}. *F - I*: Expanded stimulated twitches and DADs upon returning to normal pH_i from records *B - E*. *F* and *G* show that while in the first normal stimulated twitch, the sequence of events is: upstroke of AP, activation of I_{CaL}, activation of I_{rel}, increase in $[Ca^{2+}]_c$ and activation of I_{NCXdir}, in the DAD_{AP}, the activation of I_{rel}, the increase in $[Ca^{2+}]_c$ and the activation of I_{NCXdir} precede the depolarization. When the depolarization reaches the level of generating I_{Na} a DAD_{AP} occurs with simultaneous I_{CaL}. A DAD_{ST} is generated in *H* and *I* without I_{Na} and I_{CaL} because depolarization did not reach the threshold to elicit a DAD_{AP}. Arrows indicate the rise in diastolic $[Ca^{2+}]_c$, which is steeper (y = 1.97. time−12.0, r = 0.99) in a DAD_{AP} than in a DAD_{ST} (y = 1.77. time−17.5, r = 0.99). Vertical marks indicate stimuli. Scale range and units are indicated in brackets. See Non-standard abbreviations.

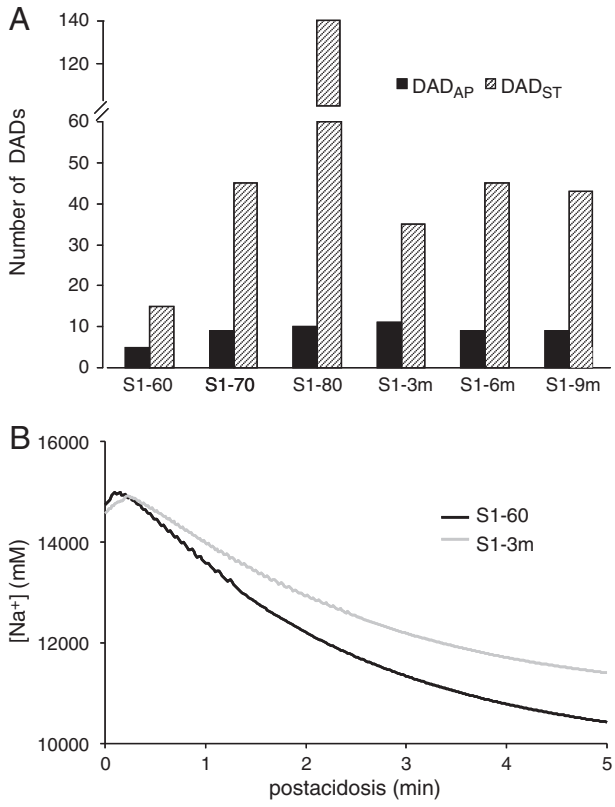

Fig. 5. Effect of PF and acidosis duration on DAD occurence in the S1 protocol. *A*: The number of DAD_{AP} occurring during the return to normal pH_i was only slightly affected by PF and acidosis duration. In contrast, PF markedly affected the number of DAD_{ST} while acidosis duration had less impact. *B*: $[Na^+]_i$ decrease from the end of acidosis to the completion of the simulation period. For a similar $[Na^+]_i$ level achieved at the end of the acidotic period either with PF or with the duration of acidosis (S1–60 and S1–3 m), there was a greater number of DADs associated with a lower rate of $[Na^+]_i$ decline during the postacidotic period. Abbreviations as in Fig. 2.

CaMKII drives L-type Ca^{2+} channels into an active gating mode with frequent, prolonged openings and is responsible for dynamically increasing I_{CaL}, a phenomenon termed facilitation [43,44]. Enhanced I_{CaL} may favor the prolongation of APD, predisposing to early after depolarizations, and the increased SR Ca^{2+} loading [45]. At the SR level, CaMKII also phosphorylates Thr17 site of PLN and Ser2814 site of RyR2 [24,26,46]. By these phosphorylations, CaMKII increases SR Ca^{2+} loading and SR Ca^{2+} leak [47]. These events working together may give rise to activation of the direct mode of the NCX inducing membrane spontaneous depolarization (DADs) [45,48].

Previous experiments from our and other laboratories [6,8] have shown that after acidotic arrhythmias are dependent on the activation of CaMKII. Moreover, experimental and modeling evidence suggest that CaMKII phosphorylation of L-type Ca^{2+} channels and PLN partially compensate for the inhibitory effect of acidosis [4,6,28]. Therefore, these and the reported CaMKII effects on RyR2, NHE, I_{to} and late I_{Na} were incorporated into our myocyte model [24–27]. This model allowed reproduction of experimental arrhythmias after a 6 min period of hypercapnic acidosis.

The mechanisms involved in after acidotic arrhythmogenesis might be explained by changes in $[Na^+]_i$ and $[Ca^{2+}]_i$ and ion flow behavior as depicted in Fig. 7. Preacidotic conditions are shown in Fig. 7A. During acidosis (Fig. 7B), there is a rise in $[Ca^{2+}]_i$ which may be partially attributed to the decrease in Ca^{2+} myofilament responsiveness together with I_{NCX} inhibition. Since CaMKII partially offsets the effect of acidosis on I_{up} but only slightly compensates the acidosis-induced reduction on I_{rel} ($I_{rel} = I_{release} + I_{leak}$), Ca^{2+} accumulates in the SR [6,14]. At a certain point, $[Ca^{2+}]_{SR}$ is high enough to overcome in part the acidosis-induced RyR2 decreased activity. These events, together with the increased $[Ca^{2+}]_i$, which reduces I_{xfer}, would produce a slight increase in $[Ca^{2+}]_c$. Increased $[Ca^{2+}]_i$ restores force to some extent as well as promotes a certain Ca^{2+} extrusion and Na^+ entry through the acidosis-inhibited I_{NCXdir}. Moreover, reduced I_{NaK}, increased late I_{Na} and enhanced I_{NHE} activity, also contribute to the increase in $[Na^+]_i$ as acidosis progresses.

During the return toward normal pH_i (Fig. 7C), there is a relief of the previous acidosis-induced inhibition on all ion flows. Recovery of I_{rel} increases I_{leak} from the overloaded SR producing a rise in $[Ca^{2+}]_c$. Similar to the mechanism postulated by Fink et al. [49], accumulation of Ca^{2+} in the DC can reach a level high enough to produce Ca^{2+} induced Ca^{2+} release, further increasing $[Ca^{2+}]_c$, I_{xfer} and hence $[Ca^{2+}]_i$. The ensuing $[Ca^{2+}]_i$ would promote its interchange by Na^+ through I_{NCXdir}, despite elevated $[Na^+]_i$, producing DADs as postulated by others [48,50]. When DADs reach the threshold of fast Na^+ channel opening, DAD_{AP} are elicited. As pH_i reaches its normal value (Fig. 7D), $[Na^+]_i$ is still high while $[Ca^{2+}]_{SR}$ and $[Ca^{2+}]_i$ have returned to near preacidotic values. This increased $[Na^+]_i$ promotes higher I_{NCXrev}, enhancing $[Ca^{2+}]_i$, I_{up}, $[Ca^{2+}]_{SR}$ and hence I_{leak} that, by increasing $[Ca^{2+}]_c$ induces Ca^{2+} induced Ca^{2+} release. In this case, however, the resulting $[Ca^{2+}]_i$ is not high enough to produce the rise in $[Na^+]_i$ that promotes fast Na^+ channel opening, and consequently DAD_{ST} are generated. As $[Na^+]_i$ starts to decrease, there is less interchange through I_{NCXrev}, and thus less Ca^{2+} is reuptaken by the SR. Therefore, several twitches are needed to progressively increase $[Ca^{2+}]_{SR}$ and Ca^{2+} leak triggering DAD_{ST} (Fig. 4A). These DAD_{ST} continue until $[Na^+]_i$ approaches its preacidotic value. A similar DAD Na^+ dependence was also observed with increased PF (Fig. 5B), in line with studies indicating elevated Na^+-induced arrhythmia occurrence [51–53].

The model thus suggests that DAD generation requires a functional SR. The present findings confirm the conclusion of our previous experimental work, where complete abrogation of arrhythmic events due to SR inhibition indicated the necessary contribution of this organelle in the arrhythmogenic pattern observed after acidosis [6]. Furthermore, the model ratifies that the SR is necessary even in the presence of an activated CaMKII. Interestingly, the model further reveals that SR Ca^{2+} load and post acidosis arrhythmias appear to be sustained by increased $[Na^+]_i$. This prediction was confirmed by experimental results in which the situation of SR $[Ca^{2+}]_i$ load and increased $[Na^+]_i$ was mimicked (Fig. 6D).

4.1. Effects of CaMKII on DADs upon returning to normal pH_i

The role of CaMKII in DAD generation can be explained by the S2 protocol where its compensatory effect on all flows was eliminated. As in this case I_{CaL} is reduced by acidosis, there is less extracellular Ca^{2+} input. In addition, because I_{up} is also decreased, there is less Ca^{2+} reuptaken by the SR, leading to reduced Ca^{2+} leak and low $[Ca^{2+}]_c$. The combination of these factors together with a greater RyR2 inhibition produces decreased $[Ca^{2+}]_i$ at the end of acidosis. The absence of CaMKII compensation on I_{NHE}, late I_{Na} as well as the decreased activity of I_{NCXdir} as a result of reduced $[Ca^{2+}]_i$, leads to lower $[Na^+]_i$ than in S1. Therefore, due to low $[Ca^{2+}]_{SR}$ and the modest rise in $[Na^+]_i$ there are no DADs after acidosis. The comparative analysis of CaMKII effects indicates that I_{CaL} (S4 protocol), and I_{up} (S5 protocol) are the main contributors to CaMKII arrhythmia promotion, indicating that both these mechanisms are necessary to reload the SR.

4.2. Model assumptions and limitations

In the present approach, we followed as closely as possible the TP myocyte model, introducing acidosis effects on I_{CaL}, I_{NaK}, I_{K1}, I_{to}, PP1

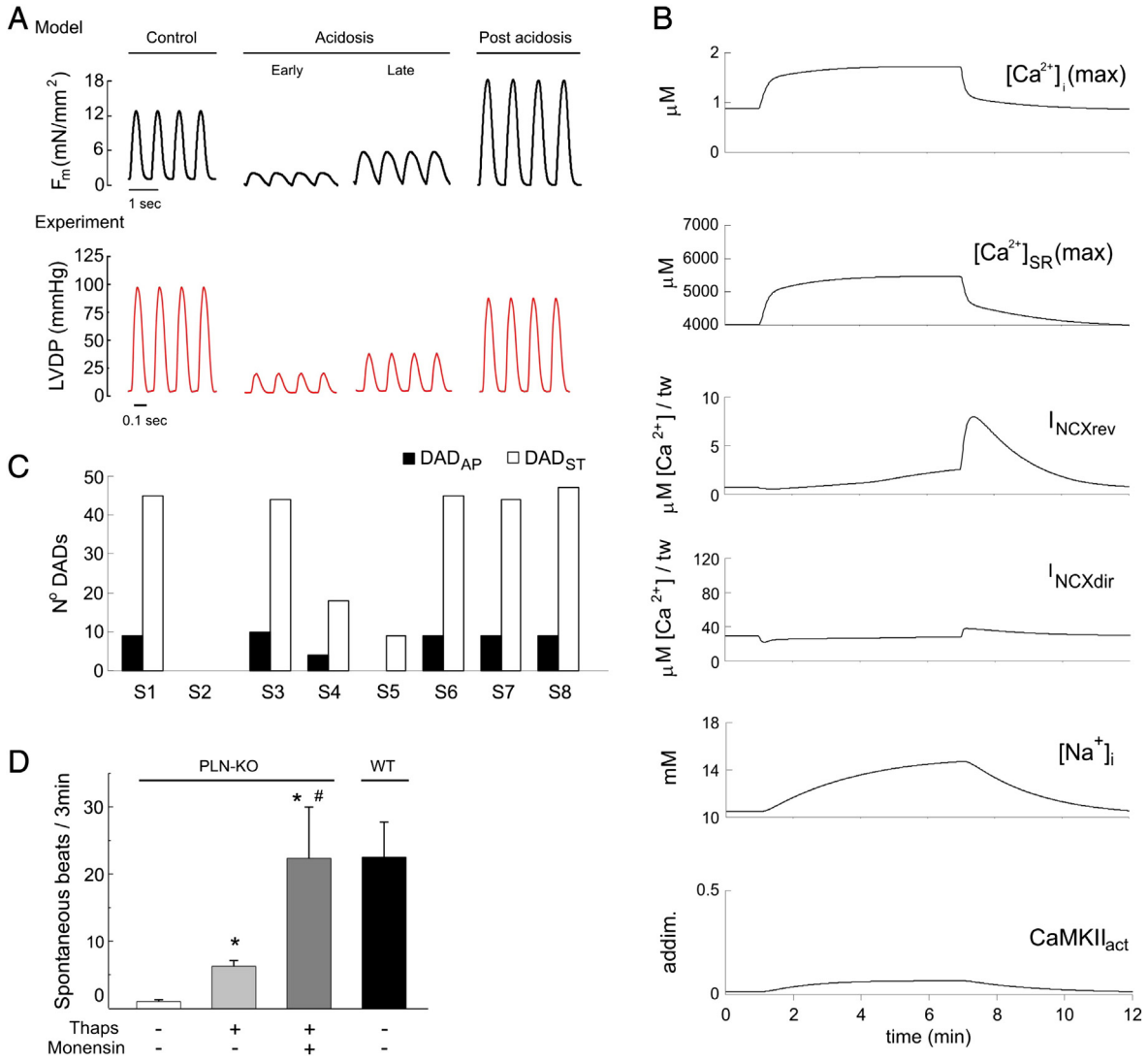

Fig. 6. (*A–C*). Effect of CaMKII on DAD generation. *A*: Comparison of model developed F_m in the absence of CaMKII effect on flows (S2 protocol) and experimental LVDP in Langendorff perfused rat heart (PF = 240 beats/min) in the presence of CaMKII inhibition with 1 μM KN-93 [6] during control, early and late acidosis and post acidosis. *B*: Effect of CaMKII inhibition on $[Ca^{2+}]_i$(max), $[Ca^{2+}]_{SR}$(max), I_{NCXrev}, I_{NCXdir}, $[Na^+]_i$ and $CaMKII_{act}$. *C*: Number of DAD_{AP} and DAD_{ST} in the different simulated protocols without CaMKII effect on specific targets as described in Methods. CaMKII inhibition abrogated arrhythmia occurrence (S2 protocol). Furthermore, CaMKII effects on I_{CaL} (S4 protocol), and I_{up} (S5 protocol) are the main contributors to CaMKII arrhythmia promotion. *D*: Experimental confirmation of model predictions. Spontaneous beats in isolated perfused PLN-KO mice in the absence and presence of thapsigargin (100 nM) and monensin (5 μM) compared to spontaneous beats in WT mice after acidosis. Mean ± SE $^*p < 0.05$ vs. PLN-KO, $^\#p < 0.05$ vs. PLN-KO + Thaps. Abbreviations as in Fig. 2.

and contractile constants in addition to those postulated by Crampin [28] on I_{rel}, I_{up}, I_{NCX}, I_{AE}, I_{NBC} and I_{NHE}. Because it has been shown that CaMKII activity is enhanced during acidosis [6,8], CaMKII effect on I_{rel}, I_{up}, I_{CaL}, I_{NHE}, I_{to} and late I_{Na} was incorporated, adopting Chiba´s scheme of CaMKII activation and O´Hara´s approach of CaMKII effect on specific targets [33,34]. A main assumption introduced in the model, considered essential for spontaneous depolarizing activity, was the incorporation of SR Ca^{2+} leak to the DC as part of RyR2 kinetics, through the resting R state of this channel. Although experimental studies have suggested spontaneous diastolic Ca^{2+} leak through the RyR2 [32,54], most previous models have postulated Ca^{2+} leak as a separate entity from the RyR2 either to the cytoplasm or DC [29,31,34,55], or as part of increased RyR2 activity, without a defined diastolic Ca^{2+} leak mechanism [56]. Only the present model, and not other human myocyte models [34,55] were able to reproduce postacidotic DADs. Although the reason for this is unclear, we believe that differences in Ca^{2+} leak management, as lack of diastolic Ca^{2+} release [34] or the inclusion of a passive SR Ca^{2+} leak to the cleft space as a separate entity from the RyR2 [55] could account for their lack of postacidotic arrhythmic response.

The representation of leak adopted in the present model was based on our previous modeling attempts showing that Ca^{2+} leak to the cytoplasm did not produce postacidotic DADs, whereas incorporation in the TP model of a RyR2-independent constant Ca^{2+} leak to the DC resulted in reduced postacidotic DADs. Moreover, Ca^{2+} leak modulated by one of the RyR2 states emerges as a more physiological description of SR Ca^{2+} regulation, resulting in extrapolated values at model $[Ca^{2+}]_{SR}$ similar to those reported experimentally [32].

The explanation of DAD generation associated to SR Ca^{2+} overload and Ca^{2+} leak differs from a recent model in normoacidotic conditions in which DADs were related to CaMKII-mediated RyR2 hyperphosphorylation [50], since our previous experiments failed to detect any significant increase in RyR2 phosphorylation either during or upon returning from acidosis [6]. However, because RyR2 is a

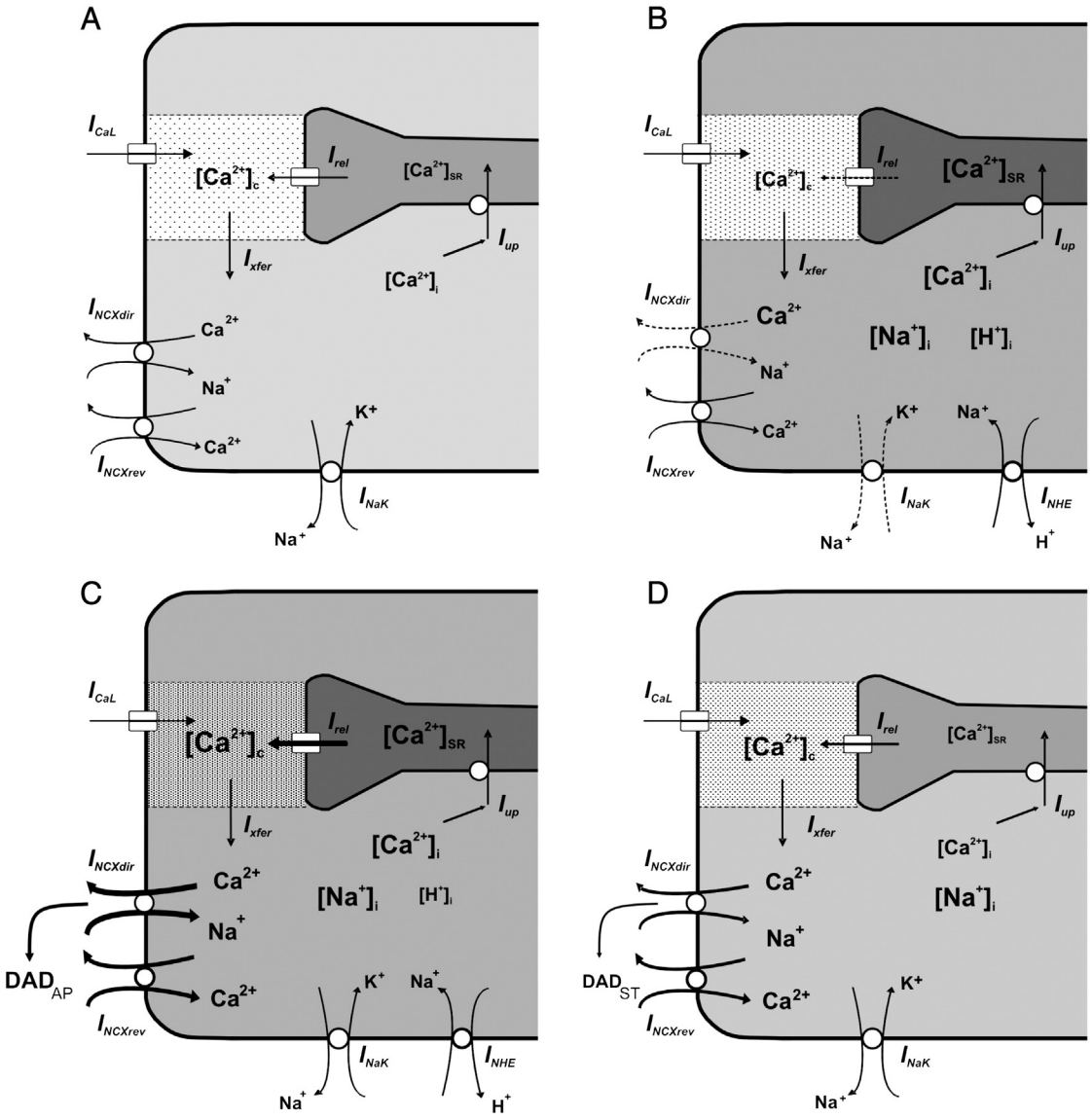

Fig. 7. Schematic representation of the different mechanisms contributing to the generation of DADs after acidosis. In *A* to *D*, different concentrations of $[Ca^{2+}]$, $[Na^+]$ and $[H^+]$ in the various compartments (SR, DC and CYTO) are denoted by the different size of the symbols and in the case of $[Ca^{2+}]$ also by the degree of shading of the compartments. Different activities of ion transporters are represented by the thickness of the arrows. The activation of NHE is indicated only in the periods in which it is relevant. Acidosis-induced inhibition in the absence of compensation is indicated by dashed lines. *A.* Preacidosis. *B.* Acidosis: At the end of the acidotic period Ca^{2+} increases in the different compartments. There is also increased $[Na^+]_i$ due to enhanced NHE activity and NaK pump inhibition. The increase in $[Na^+]_i$ produced increased I_{NCXrev}. *C.* Early post acidosis: The return to normal pH_i relieves I_{rel} and I_{NCX} from acidosis-induced inhibition. The relief of I_{rel} from an overloaded SR leads, through the activation of I_{NCXdir}, to the generation of DAD_{AP}. *D.* Late post acidosis: SR Ca^{2+} load attains near normal values. The increased $[Na^+]_i$ promotes the activation of I_{NCXrev} which, by reloading in successive twitches the SR promotes an I_{rel} that, although of lower magnitude than in C, produces DAD_{ST}. See Non-standard abbreviations and Fig. 2 abbreviations.

well-known substrate of CaMKII, we assumed a small effect of this kinase producing a slight compensation on I_{rel} inhibition, which nevertheless had scarce effect on overall DAD generation.

NCX has been found to be located in the vicinity of RyR2 [57,58], and in myocyte models this has been interpreted as 11% NCXs operating in the DC [31,55]. In our model, I_{NCX} was located outside the DC with 2.5 sensitivity amplification as in the TP model, to account for higher concentration of Ca^{2+} in the vicinity of the DC [59]. With this assumption the model revealed that NCX plays a crucial role in eliciting postacidotic DADs.

One of the model's limitations is the inadequate response of peak Ca^{2+} at low PF [60], compared to experimental data [61,62]. However, normalized model data using PFs within the range of human heart rate, evidenced an acceptable response with respect to the experimental results (Fig. SM3).

The present model provides a consistent framework to explain postacidotic arrhythmias reproducing the reported arrhythmic behavior on the return from acidosis under different experimental conditions. According to the model, two mechanisms were found to trigger spontaneous activity: an overloaded SR and a high level of $[Na^+]_i$. Both mechanisms rely on CaMKII effect on flows and SR loading and release. The model suggests for the first time that although SR Ca^{2+} overload is a well known mechanism to elicit arrhythmias, increased $[Na^+]_i$ is a critical determinant of SR reloading and hence DAD maintenance.

Disclosure statement

None declared.

Appendix A

Table A1
fh parameters f_0, n and pK for pH_i targets.

pH_i target	f_0	n	pK	*fh* (at $pH_i = 6.7$)	Reference
I_{CaL}	1.11	1.53	6.52	0.720	[4]
I_{rel}	1.11	1.87	6.64	0.627	[28]
I_{up}	3.71	1.14	7.53	0.377	[28]
I_{NCX}	2.65	0.99	7.37	0.472	[28]
I_{NaK}	1.43	−0.86	6.72	0.7	[16]
I_{K1}	1.43	−1.41	6.89	0.5	[21]
I_{to}	1.43	−0.86	6.72	0.7	[22]
I_{NHE}	40	−3.54	6.70	20	[28]
I_{AE}	146	5.11	7.57	0.547	[28]
I_{NBC}	16.8	−2.91	6.74	9.469	[28]
PP1	1.45	0.63	6.60	0.777	[35]
Y_p	1.02	4.8	6.8	0.254	[2]
Y_b	1.02	4.8	6.8	0.254	[2]
Z_b	1.02	−4.8	6.8	0.767	[2]

Calculated *fh* at pH = 6.7 illustrates acidosis effect on each pH_i target. Notice that acidosis only increased I_{NHE} and I_{NBC}.

Non-standard abbreviations

I_{Kr}	Rapid delayed rectifier flow
I_{Ks}	Slow delayed rectifier flow
I_{K1}	Inward rectifier K^+ flow
I_{Kp}	Plateau K^+ flow
I_{to}	Transient outward K^+ flow
I_{NaK}	Na^+–K^+ pump flow
I_{Na}	Fast Na^+ flow
I_{Nab}	Background Na^+ flow
I_{CaL}	L-type Ca^{2+} channel flow
I_{Cap}	Sarcolemmal Ca^{2+} pump flow
I_{Cab}	Background Ca^{2+} flow
I_{NCX}	Na^+–Ca^{2+} exchanger flow
I_{NCXdir}	Direct mode of Na^+–Ca^{2+} exchanger Ca^{2+} transport
I_{NCXrev}	Reverse mode of Na^+–Ca^{2+} exchanger Ca^{2+} transport
I_{rel}	Ca^{2+} release flow from the ryanodine receptor (RyR2)
I_{xfer}	Ca^{2+} translocation flow from DC to CYTO
I_{up}	SR Ca^{2+} reuptake pump (SERCA2a)
I_{NHE}	Na^+–H^+ exchanger flow
I_{NBC}	Na^+–HCO_3^- cotransporter flow
I_{CHE}	Cl^-–OH^- exchanger flow
I_{AE}	Cl^-–HCO_3^- exchanger flow
TS	Troponin system (= 3 regulatory units)
$TSCa_3$	Troponin system with three bound Ca^{2+}
$TSCa_3$~	$TSCa_3$ with three bridges bound in the weak state
$TSCa_3$*	$TSCa_3$ with three bridges bound in the power state
Y_b, Z_b, Y_p, Z_p, Y_r, Z_r	Reaction constants for the contractile part
f, g, g_d	Functions in the contractile part

Appendix B. Supplementary data

Supplementary data to this article can be found online at http://dx.doi.org/10.1016/j.yjmcc.2013.04.018.

References

[1] Fabiato A, Fabiato F. Effects of pH on the myofilaments and the sarcoplasmatic reticulum of skinned cells from cardiac and skeletal muscles. J Physiol 1978;276:233–55.
[2] Orchard CH, Kentish JC. Effects of changes of pH on the contractile function of cardiac muscle. Am J Physiol Cell Physiol 1990;258:C967–81.
[3] Hulme JT, Orchard CH. Effect of acidosis on Ca^{2+} uptake and release by sarcoplasmic reticulum of intact rat ventricular myocytes. Am J Physiol Heart Circ Physiol 1998;275:H977–87.
[4] Komukai K, Pascarel C, Orchard CH. Compensatory role of CaMKII on I_{Ca} and SR function during acidosis in rat ventricular myocytes. Pflugers Arch 2001;42:353–61.
[5] Vaughan-Jones RD, Spitzer KW. Role of bicarbonate in the regulation of intracellular pH in the mammalian ventricular myocyte. Biochem Cell Biol 2002;80:579–96.
[6] Said M, Becerra R, Palomeque J, Rinaldi M, Kaetzel MA, Diaz-Sylvester PL, et al. Increased intracellular Ca^{2+} and SR Ca^{2+} load contribute to arrhythmias after acidosis in rat heart. Role of Ca^{2+}/calmodulin-dependent protein kinase II. Am J Physiol Heart Circ Physiol 2008;295:H1669–83.
[7] Orchard CH, Cingolani HE. Acidosis and arrhythmias in cardiac muscle. Cardiovasc Res 1994;28:1312–9.
[8] Nomura N, Satoh H, Terada H, Matsunaga M, Watanabe H, Hayashi H. CaMKII-dependent reactivation of SR Ca^{2+} uptake and contractile recovery during intracellular acidosis. Am J Physiol Heart Circ Physiol 2002;283:H193–203.
[9] Pedersen TH, Gurung IS, Grace A, Huang CLH. Calmodulin kinase II initiates arrhythmogenicity during metabolic acidification in murine hearts. Acta Physiol 2009;197:13–25.
[10] Allen DG, Orchard CH. The effects of changes of pH on intracellular calcium transients in mammalian cardiac muscle. J Physiol 1983;335:555–67.
[11] Cairns SP, Westerblad H, Allen DG. Changes in myoplasmic pH and calcium concentration during exposure to lactate in isolated rat ventricular myocytes. J Physiol 1993;464:561–74.
[12] Choi HS, Trafford AW, Orchard CH, Eisner DA. The effect of acidosis on systolic Ca^{2+} and sarcoplasmic reticulum calcium content in isolated rat ventricular myocytes. J Physiol 2000;529:661–8.
[13] Pérez G, Mattiazzi A, Cingolani HE. Role of Na^+/H^+ exchange in the recovery of contractility during hypercapnia in cat papillary muscles. Arch Int Physiol Biochim 1993;101:107–12.
[14] Mundiña-Weilenmann C, Said M, Ferrero P, Vittone L, Kranias E, Mattiazzi A. Role of phosphorylation of Thr^{17} of phospholamban in the mechanical recovery from hypercapnic acidosis. Cardiovasc Res 2005;66:114–22.
[15] Leem CH, Lagadic-Gossmann D, Vaughan-Jones RD. Characterization of intracellular pH regulation in the guinea-pig ventricular myocyte. J Physiol 1999;517:159–80.
[16] Bielen FV, Bosteels S, Verdonck F. Consequences of CO_2 acidosis for transmembrane Na^+ transport and membrane current in rabbit cardiac Purkinje fibres. J Physiol 1990;427:325–45.
[17] ten Hove M, van Emous JG, van Echteld CJA. Na^+ overload during ischemia and reperfusion in rat hearts: comparison of the Na^+/H^+ exchange blockers EIPA, cariporide and eniporide. Mol Cell Biochem 2003;250:47–54.
[18] Irisawa H, Sato R. Intra- and extracellular actions of proton on the calcium current of isolated guinea pig ventricular cells. Circ Res 1986;59:348–55.
[19] Balnave CD, Vaughan-Jones RD. Effect of intracellular pH on spontaneous Ca^{2+} sparks in rat ventricular myocytes. J Physiol 2000;528:25–37.
[20] Terracciano CMN, MacLeod KT. Effects of acidosis on Na^+/Ca^{2+} exchange and consequences for relaxation in guinea pig cardiac myocytes. Am J Physiol Heart Circ Physiol 1994;267:H477–87.
[21] Harvey RD, Ten Eick RE. On the role of sodium ions in the regulation of the inward-rectifying potassium conductance in cat ventricular myocytes. J Gen Physiol 1989;94:329–48.
[22] Du Z, Chaoqian X, Shan H, Lu Y, Ren N. Functional impairment of cardiac transient outward K^+ current as a result of abnormally altered cellular environment. Clin Exp Pharmacol Physiol 2007;34:148–52.
[23] Witcher DR, Kovacs RJ, Schulmans H, Cefali DC, Jones LR. Unique phosphorylation site on the cardiac ryanodine receptor regulates calcium channel activity. J Biol Chem 1991;266:11144–52.
[24] Ferrero P, Said M, Sánchez G, Vittone L, Valverde C, Donoso P, et al. Ca^{2+}/calmodulin kinase II increases ryanodine binding and Ca^{2+}-induced sarcoplasmic reticulum Ca^{2+} release kinetics during β-adrenergic stimulation. J Mol Cell Cardiol 2007;43:281–91.
[25] Vila-Petroff M, Mundiña-Weilenmann C, Lezcano N, Snabaitis AK, Huergo MA, Valverde CA, et al. Ca^{2+}/calmodulin dependent protein kinase II contributes to intracellular pH recovery from acidosis via Na^+/H^+ exchanger activation. J Mol Cell Cardiol 2009;49:106–12.
[26] Wagner S, Hacker E, Grandi E, Weber SL, Dybkova N, Sossalla S, et al. Ca/calmodulin kinase II differentially modulates potassium currents. Circ Arrhythm Electrophysiol 2009;2:285–94.
[27] Wagner S, Dybkova N, Rasenack ECL, Jacobshagen C, Fabritz L, Kirchhof P, et al. Ca^{2+}/calmodulin-dependent protein kinase II regulates cardiac Na^+ channels. J Clin Invest 2006;116:3127–38.
[28] Crampin EJ, Smith NP. A dynamic model of excitation-contraction coupling during acidosis in cardiac ventricular myocytes. Biophys J 2006;90:3074–90.
[29] ten Tusscher KHWJ, Panfilov AV. Alternans and spiral breakup in a human ventricular tissue model. Am J Physiol Heart Circ Physiol 2006;291:H1088–100.
[30] Negroni JA, Lascano EC. Simulation of steady state and transient cardiac muscle response experiments with a Huxley-based contraction model. J Mol Cell Cardiol 2008;45:300–12.
[31] Shannon TR, Wang F, Puglisi J, Weber C, Bers DM. A mathematical treatment of integrated Ca dynamics within the ventricular myocyte. Biophys J 2004;87:3351–71.
[32] Shannon TR, Ginsburg KS, Bers DM. Quantitative assessment of the SR Ca^{2+} leak–load relationship. Circ Res 2002;91:594–600.
[33] Chiba H, Schneider NS, Matsuoka S, Noma A. A simulation study on the activation of cardiac CaMKII δ-isoform and its regulation by phosphatases. Biophys J 2008;95:2139–49.

[34] O'Hara T, Virág L, Varró A, Rudy Y. Simulation of the undiseased human cardiac ventricular action potential: model formulation and experimental validation. PLoS Comput Biol 2011;7:e1002061.
[35] Mundiña-Weilenmann C, Vittone L, Cingolani HE, Orchard CH. Effects of acidosis on phosphorylation of phospholamban and troponin I in rat cardiac muscle. Am J Physiol Cell Physiol 1996;270:C107–14.
[36] Luo W, Grupp IL, Harrer J, Ponniah S, Grupp G, Duffy JJ, et al. Targeted ablation of the phospholamban gene is associated with markedly enhanced myocardial contractility and loss of beta-agonist stimulation. Circ Res 1994;75:401–9.
[37] Pérez NG, Mattiazzi AR, Camilión de Hurtado MC, Cingolani HE. Myocardial contractility recovery during hypercapnic acidosis: its dissociation from recovery in pHi by ryanodine. Can J Cardiol 1995;11:553–60.
[38] Bethell HWL, Vandenberg JI, Smith GA, Grace AA. Changes in ventricular repolarization during acidosis and low-flow ischemia. Am J Physiol Heart Circ Physiol 1998;275:H551–61.
[39] Brittsan AG, Carr AN, Schmidt AG, Kranias EG. Maximal inhibition of SERCA2 Ca^{2+} affinity by phospholamban in transgenic hearts overexpressing a non-phosphorylatable form of phospholamban. J Biol Chem 2000;275:12129–35.
[40] Carmeliet E. Cardiac ionic currents and acute ischemia: from channels to arrhythmias. Physiol Rev 1999;79:917–1017.
[41] Keating MT, Sanguinetti MC. Molecular and cellular mechanisms of cardiac arrhythmias. Cell 2001;104:569–80.
[42] Anderson ME. Calmodulin kinase signalling in heart: an intriguing candidate target for therapy of myocardial dysfunction and arrhythmias. Pharmacol Ther 2005;106:39–55.
[43] Yuan W, Bers DM. Ca-dependent facilitation of cardiac Ca current is due to Ca-calmodulin dependent protein kinase. Am J Physiol Heart Circ Physiol 1994;267:H982–93.
[44] Wu Y, MacMillan LB, McNeill RB, Colbran RJ, Anderson ME. CaM kinase augments cardiac L-type Ca^{2+} current: a cellular mechanism for long Q-T arrhythmias. Am J Physiol Heart Circ Physiol 1999;276:H2168–78.
[45] Wu Y, Roden DM, Anderson ME. Calmodulin kinase inhibition prevents development of the arrhythmogenic transient inward current. Circ Res 1999;84:906–12.
[46] Mundiña-Weilenmann C, Vittone L, Ortale M, Chiappe de Cingolani G, Mattiazzi A. Immunodetection of phosphorylation sites gives new insights into the mechanisms underlying phospholamban phosphorylation in the intact heart. J Biol Chem 1996;271:33561–7.
[47] Maier LS, Zhang T, Chen L, DeSantiago J, Brown JH, Bers DM. Transgenic CaMKIIdeltaC overexpression uniquely alters cardiac myocyte Ca^{2+} handling: reduced SR Ca^{2+} load and activated SR Ca^{2+} release. Circ Res 2003;92:904–11.
[48] Pogwizd SM, Schlotthauer K, Li L, Yuan W, Bers DM. Arrhythmogenesis and contractile dysfunction in heart failure: roles of sodium-calcium exchange, inward rectifier potassium current, and residual beta-adrenergic responsiveness. Circ Res 2001;88:1159–67.
[49] Fink M, Noble PJ, Noble D. Ca^{2+}-induced delayed afterdepolarizations are triggered by dyadic subspace Ca^{2+} affirming that increasing SERCA reduces aftercontractions. Am J Physiol Heart Circ Physiol 2011;301:H921–35.
[50] Soltis AR, Saucerman JJ. Synergy between CaMKII substrates and β-adrenergic signaling in regulation of cardiac myocyte Ca^{2+} handling. Biophys J 2010;99:2038–47.
[51] Pike MM, Luo CS, Yanagida S, Hageman GR, Anderson PG. ^{23}Na and ^{31}P nuclear magnetic resonance studies of ischemia-induced ventricular fibrillation. Alterations of intracellular Na^+ and cellular energy. Circ Res 1995;77:394–406.
[52] Satoh H, Ginsburg KS, Qing K, Terada H, Hayashi H, Bers DM. KB-R7943 block of Ca^{2+} influx via Na^+/Ca^{2+} exchange does not alter twitches or glycoside inotropy but prevents Ca^{2+} overload in rat ventricular myocytes. Circulation 2000;101:1441–6.
[53] Sedej S, Heinzel FR, Walther S, Dybkova N, Wakula P, Groborz J, et al. Na^+-dependent SR Ca^{2+} overload induces arrhythmogenic events in mouse cardiomyocytes with a human CPVT mutation. Cardiovasc Res 2010;87:50–9.
[54] Bassani RA, Bers DM. Rate of diastolic Ca release from the sarcoplasmic reticulum of intact rabbit and rat ventricular myocytes. Biophys J 1995;68:2015–22.
[55] Grandi E, Pasqualini FS, Bers DM. A novel computational model of the human ventricular action potential and Ca transient. J Mol Cell Cardiol 2010;48:112–21.
[56] Hashambhoy YL, Greenstein JL, Winslow RL. Role of CaMKII in RyR leak, EC coupling and action potential duration: a computational model. J Mol Cell Cardiol 2010;49:617–24.
[57] Lakatta EG, Maltsev VA, Vinogradova TM. A coupled system of intracellular Ca^{2+} clocks and surface membrane voltage clocks controls the timekeeping mechanism of the heart's pacemaker. Circ Res 2010;106:659–73.
[58] Langer GA, Peskoff A. Calcium concentration and movement in the dyadic cleft space of the cardiac ventricular cell. Biophys J 1996;70:1169–82.
[59] ten Tusscher KHWJ, Noble D, Noble PJ, Panfilov AV. A model for human ventricular tissue. Am J Physiol Heart Circ Physiol 2004;286:H1573–89.
[60] Romero L, Pueyo E, Fink M, Rodriguez B. Impact of ionic current variability on human ventricular cellular electrophysiology. Am J Physiol Heart Circ Physiol 2009;297:H1436–45.
[61] Pieske B, Kretschmann B, Meyer M, Holubarsch C, Weirich J, Posival H, et al. Alterations in intracellular calcium handling associated with the inverse force-frequency relation in human dilated cardiomyopathy. Circulation 1995;92(5):1169–78.
[62] Schmidt U, Hajjar RJ, Helm PA, Kim CS, Doye AA, Gwathmey JK. Contribution of abnormal sarcoplasmic reticulum ATPase activity to systolic and diastolic dysfunction in human heart failure. J Mol Cell Cardiol 1998;30:1929–37.